


Revealing buckling of an apparently flat monolayer of NaCl on Pt(111)Alfred J. Weymouth^{1,*}, Mats Persson², and Franz J. Giessibl¹¹*Department of Physics, University of Regensburg, Regensburg 93053, Germany*²*Surface Science Research Centre, University of Liverpool, Liverpool L69 3BX, United Kingdom* (Received 27 November 2020; revised 28 August 2021; accepted 14 December 2021; published 11 January 2022)

Platinum is relatively reactive, compared to silver and copper, which prompted us to study the growth and structure of a thin insulating layer on Pt(111). We grew monolayer islands of NaCl and studied them with scanning tunneling microscopy (STM) and atomic force microscopy (AFM). STM images of the islands revealed a square lattice which we confirmed, via density functional theory (DFT) calculations, to be the Cl anions, similar to other surfaces. Surprisingly, however, the AFM images appeared to only resolve approximately two-thirds of the Cl ions. DFT calculations showed that the adsorption heights of the Cl anions above the surface have a bimodal distribution in which they are either approximately 60 pm above the Na ionic plane or 40 pm lower. An electrostatic model shows that this structure reproduces the AFM observations.

DOI: [10.1103/PhysRevB.105.035412](https://doi.org/10.1103/PhysRevB.105.035412)**I. INTRODUCTION**

Thin insulating films on conducting substrates are one of the most studied class of heteroepitaxial systems due to their practical importance. They allow patterning of interface states, and tailored coupling of further adsorbates to the underlying metal surface [1–5]. NaCl has been studied on various surfaces, because it is useful, easy to evaporate, and forms well-ordered monolayer and bilayer islands [6]. The scanning tunneling microscope has been key to investigating these systems, as it can directly image the atomic lattice and the orientation of individual islands with respect to the underlying substrate [7]. NaCl on Ag(111) interacts weakly, and there is no clear alignment between the orientation and the underlying substrate [8]. NaCl appears to react stronger with Cu(111) and the atomic rows of the islands align with the high-symmetry direction of the substrate [9,10].

Pt is more reactive than Ag or Cu, and is often used as a catalyst [11]. Due to strong spin-orbit coupling, it is also of interest for magnetic adsorbates [12]. The magnetic moments of transition metals in the form of single adatoms and small clusters have been studied on Pt(111) [13–15]. The interaction of one magnetic adatom with a neighbor via the platinum surface can be tuned by their distance from each other [16]. Another method to tune the interaction between the underlying metal substrate and magnetic adsorbates is via a thin insulating layer [17]. For applications both as a catalysis and as a host of magnetic adsorbates, we studied a thin (single atomic layer) insulating layer on Pt(111).

In this Letter, we study islands of NaCl on Pt(111) experimentally with scanning tunneling microscopy (STM) and atomic force microscopy (AFM), and theoretically with density functional theory (DFT) calculations. While the STM results appear similar to those previously reported of NaCl on Cu(111), with the high-symmetry direction of the island

aligned to one of the high-symmetry directions of the substrate [18], the AFM data show a more complex pattern. The Cl anions appear either bright or dark, forming patterns of polyominoes with no apparent regular long-range order. (Polyominoes are figures made by joining several squares along edges. The most popular are the “tetris blocks.”) This is in stark contrast to AFM results of NaCl on Cu(111), where the expected square lattice is observed [6,19,20].

To address whether this is an electronic or geometric effect, we performed DFT calculations. The DFT calculations show that the strong interaction of the NaCl to the substrate results in Cl anions being either in a raised or lowered state, with a height difference of 0.1 nm. This buckling, which is not visible in the STM images, is revealed clearly in the AFM images.

II. EXPERIMENTAL OBSERVATIONS

Measurements were taken at 5.8 K in a low-temperature (LT)-STM/AFM system operating in UHV (CreaTec Fischer and Company GmbH, Germany). STM and AFM data were acquired with a qPlus sensor [21] operating in frequency-modulation mode [22] oscillating at an amplitude of 50 pm. Further details are available in the Supplemental Material [23].

Figure 1(a) shows a typical overview STM image. Growth starts and naturally terminates at the step edges, as has been observed on Ag(100) [24]. The NaCl islands have an apparent height in the STM images of 0.18 nm, which corresponds to a single layer. There is no indication of carpetlike growth over a step edge as observed for growth on other surfaces [9]. STM and AFM images of one of the NaCl islands, which were acquired simultaneously at a constant height, are shown in Figs. 1(b) and 1(c). The high-conductance features in the STM image [Fig. 1(b)] form a square lattice with a lattice constant of 0.38 nm. These features correspond to the Cl anions as suggested by previous studies [25,26], which is also confirmed by our STM simulations as shown below. There

*jay.weymouth@ur.de

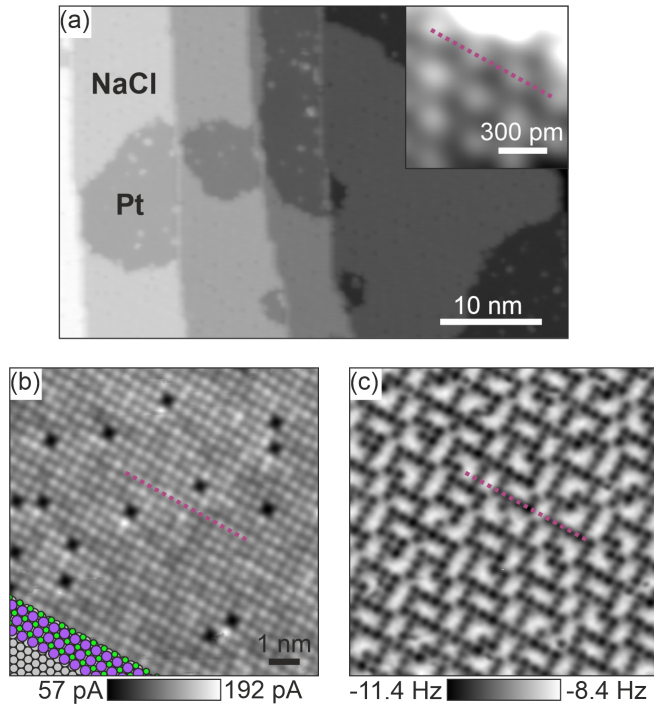


FIG. 1. (a) Overview STM image of monolayer NaCl islands on Pt(111) ($V = 500$ mV, $I = 100$ pA). Inset: Constant-height STM image of the Pt(111) surface showing atomic resolution ($V = 2$ mV, average current 1.4 nA). The purple dotted line shows one of the high-symmetry directions of the Pt(111) surface. (b) Constant-height STM image above a NaCl island with $V = 10$ mV and (c) AFM image acquired simultaneously. Purple lines in (b) and (c) are in the same orientation as the purple line in the inset of (a) showing alignment of the island with the substrate. The inset in (b) is a sketch of the Pt surface atoms as gray circles and the Na and Cl ions as green and purple, respectively.

are also several low-conductance features, which could correspond to Cl anion vacancies.

We compared the orientation of the NaCl islands to the Pt(111) surface and conclude, in agreement with Ref. [18], that one of the high-symmetry directions of the NaCl layers corresponds to one of the high-symmetry directions of the Pt(111) surface. The high-symmetry orientation of Pt substrate atoms indicated in the inset of Fig. 1(a) is aligned along one of the high-symmetry directions of the NaCl monolayer indicated in Figs. 1(b) and 1(c).

Simultaneously, we collected AFM data, shown in Fig. 1(c). In contrast to AFM images of NaCl multilayers on other metal surfaces [6,19] we do not see a lattice similar to that in the STM image, but rather a pattern of polyominoes.

There are distinct features of a lower-frequency shift Δf that have the size of one Cl anion. These atomic features are at the same positions as the high-conductance features in the STM image, leading us to conclude that they represent the negatively charged Cl anion, as expected from a positively charged metal tip [19,27,28]. If the features of low Δf are indeed the Cl anions, then it appears as though almost one-third of the Cl anions are missing in the AFM image. An analysis of the patterns over several islands indicates that the polyominoes have a size of approximately

1 nm. We were unable to identify any long-range order of the polyominoes in the images. Furthermore, the polyominoes are also roughly aligned in a rotationally threefold pattern which themselves match the underlying substrate, indicating a strong relationship between this pattern and the Pt(111) surface.

We also acquired images with a CO-terminated tip [23]. Again in the STM data all Cl anions can be observed, whereas in the AFM images only approximately one-third of them appear, but this time as higher Δf features. This reverse behavior of the AFM images for this functionalized tip compared to a metal tip is understood from AFM images of ionic surfaces with CO-terminated tips to be mainly due to the electrostatics of a negatively charged front atom of the tip, whereas a metal tip is positively charged [20,27,29].

From the images, it is unclear what kind of physical mechanism is behind the missing Cl anions in the AFM images. There are two possibilities: either an electronic structure effect where a fraction of the Cl atoms is in a different charge state than the others or a geometric effect where one fraction of the Cl anions is at a different height above the surface than the others. It is also unclear from the images why the STM does not show a similar pattern as the AFM but rather shows all Cl atoms with approximately the same intensity.

III. DFT CALCULATIONS

In order to better understand the nature of the AFM images, we modeled this system with periodic DFT calculations using VASP 5.4.4 [30] and the van der Waals functional vdW-DF-cx [31–33]. The surface supercell $\begin{pmatrix} 7 & 0 \\ -4 & 8 \end{pmatrix}$ was chosen to minimize the strain between the two incommensurate surface lattices and the rows of Cl atoms were aligned along the high-symmetry directions of the Pt surface. Since the calculated nearest-neighbor distance of Pt atoms is $d_{\text{Pt}} = 278$ pm and the calculated Cl-Cl distance of a free-standing NaCl monolayer is $d_{\text{Cl}} = 383$ pm, this surface supercell is nearly in coincidence with a (5×5) surface supercell of the NaCl monolayer: $7 \times d_{\text{Pt}} = 1.946$ nm, $4 \times \sqrt{3} \times d_{\text{Pt}} = 1.926$ nm, and $5 \times d_{\text{Cl}} = 1.915$ nm. Further details are available in the Supplemental Material [23].

The resulting geometrically relaxed structure is shown by the top and tilted views in Figs. 2(a) and 2(b), respectively. As shown by the top view, the adsorbed NaCl monolayer retains the square lattice of the free-standing monolayer while the tilted view shows that the adsorbed monolayer is strongly corrugated with the Cl anions at different heights above the Pt surface layer. This corrugation is clearly demonstrated by the distribution of the heights of the Na and Cl ions above the top layer of the Pt atoms shown in Fig. 2(c). While the Na ions all fall between 0.27 and 0.30 nm above the Pt surface layer, the Cl ions show a pronounced bimodal distribution of their heights, with almost half of them being 0.1 nm lower than the others.

The substantial different adsorption heights of the Cl atoms raises the question whether these atoms are in different charge states. A comparison of the electronic structure of the raised versus lowered Cl atoms shows they are both singly charged anions. As shown by the density of states of p waves around

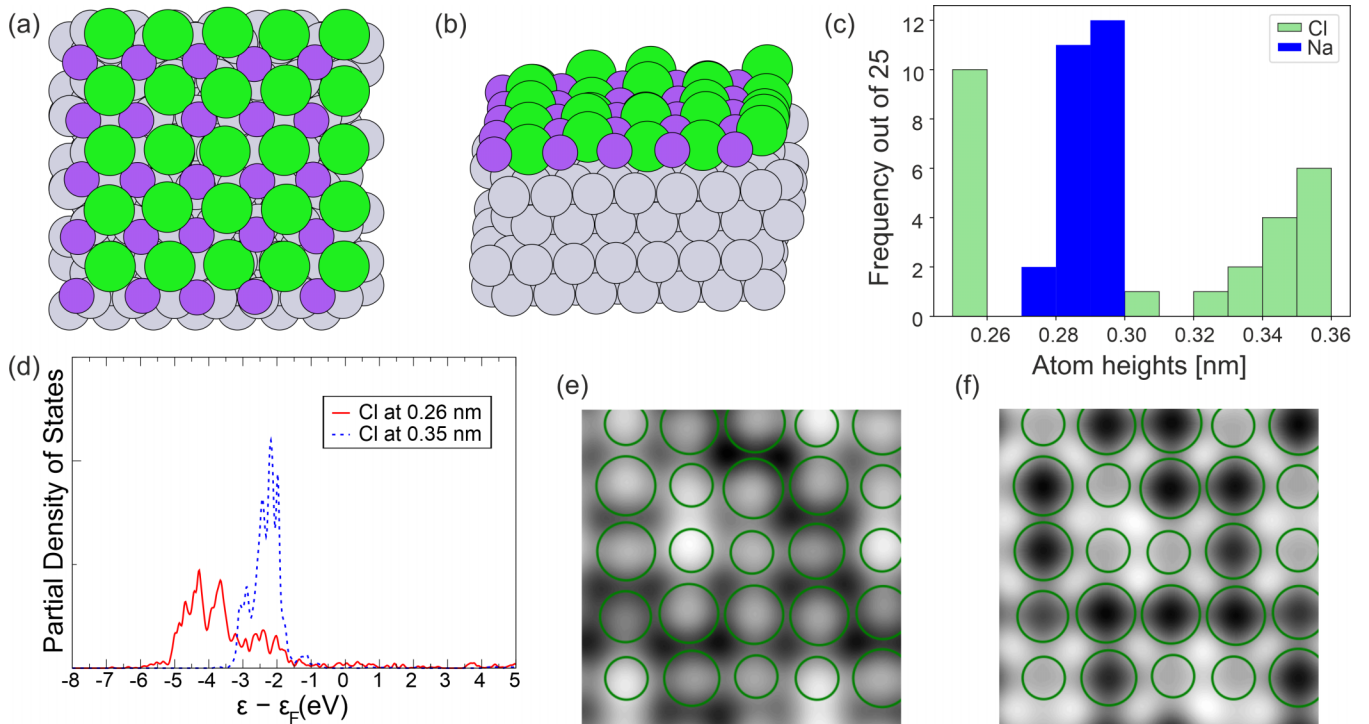


FIG. 2. DFT calculations of an NaCl monolayer on Pt(111). (a) Top and (b) tilted view of the geometrically optimized structure. Color code: Cl green; Na purple; Pt silver. (c) A histogram of ion heights above the surface. (d) Density of states of p partial waves around Cl atoms at heights of 0.26 and 0.35 nm. (e) Simulated STM image calculated by tracing the contours of the local density of states at an average height of 0.6 nm above the Pt surface. (f) Electric field calculated at a height 0.69 nm above the Pt layer. In (e) and (f), the Cl atoms are indicated by green circles with their radii being proportional to the heights of the Cl atoms above the surface.

the Cl atoms in Fig. 2(d), the p states are substantially under the Fermi level, and the p shells are fully occupied. There is an interesting difference between the raised and lowered Cl ions in that the raised Cl ion has a sharper peak that is higher in energy. This behavior is due to a decrease of their interaction with the metal substrate compared with the Cl atoms at lower heights.

In order to see how these geometrical structure effects would translate into the STM and AFM observations, we simulated both STM and AFM images. As shown by the simulated, topographical STM image in Fig. 2(e), the Cl anions show up as protrusions with various heights. However, the heights of the protrusions do not simply correlate with the heights of the Cl atoms. This behavior is due to a compensation effect of the tunneling from the tip through a Cl anion to the surface with the anion height. The increase of the height of a Cl anion by 0.1 nm increases the tunneling rate from the tip to the anion by a factor of about 10, but this increase is compensated by the decrease of the local density of states (LDOS) above the anion by a factor of about 10 [23]. The Cl anions that are 0.1 nm higher [corresponding to the second height peak in Fig. 2(e)] have a LDOS that is approximately ten times less than those that are lower, which explains why the STM images show no apparent signature of this buckling.

To further investigate the relation between the LDOS and the height of the Cl anions, we again calculated the LDOS above Cl anions when they were artificially displaced from their equilibrium position. Interestingly, the LDOS does not change monotonically as a function of distance to the Pt

surface [23]. However, when raised Cl anions are lowered or lower Cl anions are raised, the LDOS increases over them. When the anions are brought to the height of the Na plane, the LDOS above different Cl anions would be different.

In the simulation of the AFM images at 690 pm above the Pt atoms, the contrast is assumed to be due to the electrostatic interaction with the metal tip [28] through the component of the electric field in the direction of the surface normal [34]. Figure 2(f) shows this field component at a height of 0.69 nm above the Pt layer and the image exhibits similar polyominoes as in the AFM images.

As expected the field correlates with the heights of the Cl anions, since the electric field points locally towards and away from the surface for the raised and lowered Cl anions, respectively. In that sense, a resulting pattern with some Cl ions raised with respect to the Na layer and some lowered is similar to polarization compensation mechanisms that have been observed on other ionic surfaces [35]. The opposite directions of the electric field are very similar, albeit at an atomic scale, to the local polarity of positively or negatively charge islands discussed in Ref. [36].

The theoretical results were demonstrated to be quantitatively consistent with our observations by simulating the observed data based on these results and a simple electrostatic model that included a monolayer of Na and Cl ions. Those Cl ions that appeared bright in Fig. 3(a) were set at a position of -40 pm under the Na layer, while those that appeared dark in Fig. 3(a) were set at a height of 60 pm. All Cl ions were

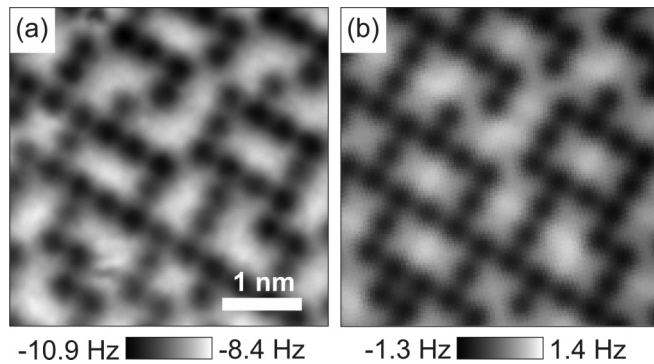


FIG. 3. (a) AFM image above a NaCl island and (b) simulated AFM image.

considered as negative point charges $-e$ and the Na ions as positive point charges $+e$. The tip was modeled as a single point charge of $0.13e$ [27,28]. The vertical component of force $F(x, y)$ and the force gradient $k_{ts}(x, y)$ were determined by finite differences of the electrostatic interaction energy between the tip and the NaCl layer at a fixed vertical distance of $z = 550$ pm. The small-amplitude approximation was then used to determine Δf [37]: $\Delta f(x, y) = \frac{f_0}{2k} k_{ts}(x, y)$. As shown in Fig. 3(b), the resulting contrast is in excellent agreement to the observed contrast in Fig. 3(a). As the long-range van der Waals forces are not included in the model, only the contrast is reproduced, not the absolute Δf values.

As can be seen in the AFM data, Figs. 1(c) and 3(a), there are certain areas with streaks in the images. These streaks can be more easily seen in the raw data [23]. Since the positions of the streaks are highly localized to single atoms, it is unlikely that they represent an instability of the tip, but rather that the vertical position of a Cl ion is unstable.

We have irregularly observed switching events both from a raised Cl ion to a lowered Cl ion and vice versa. One such event is captured by the simultaneously acquired STM and AFM images shown in Fig. 4. Here, the island terminates at the upper left-hand side of the image. Initially, a Cl ion appears raised, as indicated by the blue arrow, while a neighboring Cl ion appeared lowered, as indicated by a white arrow. Subsequent constant-height images [Figs. 4(c) and 4(d)] show that the lowered Cl ion (white arrow) is now raised, and the raised Cl ion is now lowered.

Finally, we can ask if the bimodal height distribution is a general result by calculating the heights of Cl anions in a monolayer of NaCl on Ag(111) via DFT calculations. Again, the NaCl layer is not commensurate with the Ag(111) surface, and Cl anions relax both below and above the plane of the Na cations. Similar to the Pt(111) surface, the heights of the Cl anions show a bimodal height distribution [23]. This implies

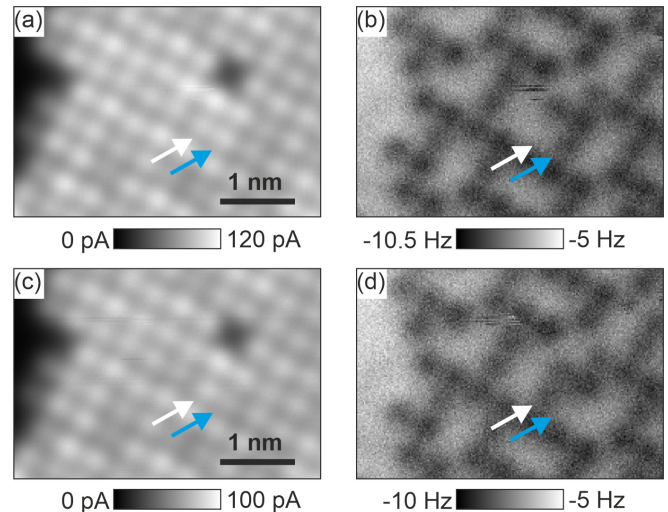


FIG. 4. Simultaneously acquired (a) STM and (b) AFM images taken at a constant height. The raised and lowered Cl ions are indicated by white and blue arrows, respectively. Corresponding (c) STM and (d) AFM images taken 43 min later at a 10 pm higher height. The Cl ion at the blue arrow is now raised while the Cl ion at the white arrow is now lowered. $V = 10$ mV for both images.

that this buckling of a monolayer NaCl on metal surfaces will be found on other surfaces as well.

IV. SUMMARY AND OUTLOOK

To summarize, we carried out a STM and AFM study of NaCl monolayer islands on a flat metal surface. As corroborated by density function theory calculations, the images exhibit a pattern of polyominoes, due to an unusual buckling effect. Understanding the strong buckling in this thin insulating layer is key to its use in future applications. The Cl ions are either above or below the plane defined by the Na ions. Certain atoms are bistable, as has been observed in NaCl layers on a $c(2 \times 2)$ N-Cu(100) surface [38]. Interestingly, the buckling does not have a strong effect on the STM signal due to a trade-off between the Cl ion height over the surface and the magnitude of the LDOS, but can be clearly seen in the AFM signal via the local electrostatic field. This local field is much different from that observed on NaCl bilayers on Cu(111) [6], and can be thought of as a tool to pattern the electric field at the atomic level, offering the possibility to pattern adsorbates on an insulating layer via the polyominoes.

ACKNOWLEDGMENT

The authors thank O. Gretz for experimental help, and J. Repp and A. Liebig for feedback on the manuscript.

- [1] J. Repp, G. Meyer, F. E. Olsson, and M. Persson, Controlling the charge state of individual gold adatoms, *Science* **305**, 493 (2004).
 [2] J. Repp, G. Meyer, S. Paavilainen, F. E. Olsson, and M. Persson, Scanning Tunneling Spectroscopy of Cl Vacancies in NaCl

- Films: Strong Electron-Phonon Coupling in Double-Barrier Tunneling Junctions, *Phys. Rev. Lett.* **95**, 225503 (2005).
 [3] C. J. Villagomez, T. Zambelli, S. Gauthier, A. Gourdon, S. Stojkovic, and C. Joachim, STM images of a large organic molecule adsorbed on a bare metal substrate or on a thin

- insulating layer: Visualization of HOMO and LUMO, *Surf. Sci.* **603**, 1526 (2009).
- [4] W. Steurer, J. Repp, L. Gross, and G. Meyer, Damping by sequentially tunneling electrons, *Surf. Sci.* **678**, 112 (2018).
- [5] F. Donati, S. Rusponi, S. Stepanow, C. Wackerlin, A. Singha, L. Persichetti, R. Baltic, K. Diller, F. Patthey, E. Fernandes, J. Dreiser, Z. Slijivancanin, K. Kummer, C. Nistor, P. Gambardella, and H. Brune, Magnetic remanence in single atoms, *Science* **352**, 318 (2016).
- [6] R. Bennewitz, A. S. Foster, L. N. Kantorovich, M. Bammerlin, C. Loppacher, S. Schar, M. Guggisberg, E. Meyer, and A. L. Shluger, Atomically resolved edges and kinks of NaCl islands on Cu(111): Experiment and theory, *Phys. Rev. B* **62**, 2074 (2000).
- [7] J. Repp, S. Folsch, G. Meyer, and K.-H. Rieder, Ionic Films on Vicinal Metal Surfaces: Enhanced Binding due to Charge Modulation, *Phys. Rev. Lett.* **86**, 252 (2001).
- [8] F. Matthaei, S. Heidorn, K. Boom, C. Bertram, A. Safiei, J. Henzl, and K. Morgenstern, Coulomb attraction during the carpet growth mode of NaCl, *J. Phys.: Condens. Matter* **24**, 354006 (2012).
- [9] R. Bennewitz, V. Barwich, M. Bammerlin, C. Loppacher, M. Guggisberg, A. Baratoff, E. Meyer, and H. J. Guntherodt, Ultrathin films of NaCl on Cu(111): A LEED and dynamic force microscopy study, *Surf. Sci.* **438**, 289 (1999).
- [10] J. Repp, G. Meyer, and K.-H. Rieder, Snell's Law for Surface Electrons: Refraction of an Electron Gas Imaged in Real Space, *Phys. Rev. Lett.* **92**, 036803 (2004).
- [11] J. Winterlin, S. Volkening, T. V. Janssens, T. Zambelli, and G. Ertl, Atomic and macroscopic reaction rates of a surface-catalyzed reaction, *Science* **278**, 1931 (1997).
- [12] P. Gambardella, S. Rusponi, M. Veronese, S. S. Dhesi, C. Grazioli, A. Dallmeyer, I. Cabria, R. Zeller, P. H. Dederichs, K. Kern, C. Carbone, and H. Brune, Giant Magnetic Anisotropy of Single Cobalt Atoms and Nanoparticles, *Science* **300**, 1130 (2003).
- [13] A. A. Khajetoorians, T. Schlenk, B. Schweflinghaus, M. dos Santos Dias, M. Steinbrecher, M. Bouhassoune, S. Lounis, J. Wiebe, and R. Wiesendanger, Spin Excitations of Individual Fe Atoms on Pt(111): Impact of the Site-Dependent Giant Substrate Polarization, *Phys. Rev. Lett.* **111**, 157204 (2013).
- [14] S. Brinker, M. dos Santos Dias, and S. Lounis, Interatomic orbital magnetism: The case of $3d$ adatoms deposited on the Pt(111) surface, *Phys. Rev. B* **98**, 094428 (2018).
- [15] M. M. Bezerra-Neto, M. S. Ribeiro, B. Sanyal, A. Bergman, R. B. Muniz, O. Eriksson, and A. B. Klautau, Complex magnetic structure of clusters and chains of Ni and Fe on Pt(111), *Sci. Rep.* **3**, 3054 (2013).
- [16] A. A. Khajetoorians, M. Steinbrecher, M. Ternes, M. Bouhassoune, M. dos Santos Dias, S. Lounis, J. Wiebe, and R. Wiesendanger, Tailoring the chiral magnetic interaction between two individual atoms, *Nat. Commun.* **7**, 10620 (2016).
- [17] C. F. Hirjibehedin, C. P. Lutz, and A. J. Heinrich, Spin coupling in engineered atomic structures, *Science* **312**, 1021 (2006).
- [18] J. Roberts, S. Hoffer, M. Van Hove, and G. Somorjai, Tensor low-energy electron diffraction analysis of the surface structure of NaCl(100) thin films grown on Pd(100) and Pt(111), *Surf. Sci.* **437**, 75 (1999).
- [19] L. Gross, B. Schuler, F. Mohn, N. Moll, N. Pavlicek, W. Steurer, I. Scivetti, K. Kotsis, M. Persson, and G. Meyer, Investigating atomic contrast in atomic force microscopy and Kelvin probe force microscopy on ionic systems using functionalized tips, *Phys. Rev. B* **90**, 155455 (2014).
- [20] M. Ellner, N. Pavlicek, P. Pou, B. Schuler, N. Moll, G. Meyer, L. Gross, R. Perez, and R. Perez, The electric field of CO tips and its relevance for atomic force microscopy, *Nano Lett.* **16**, 1974 (2016).
- [21] F. J. Giessibl, High-speed force sensor for force microscopy and profilometry utilizing a quartz tuning fork, *Appl. Phys. Lett.* **73**, 3956 (1998).
- [22] T. R. Albrecht, P. Grutter, D. Horne, and D. Rugar, Frequency modulation detection using high-Q cantilevers for enhanced force microscope sensitivity, *J. Appl. Phys.* **69**, 668 (1991).
- [23] See Supplemental Material at <http://link.aps.org/supplemental/10.1103/PhysRevB.105.035412> for further experimental and theoretical details, images with a CO tip, raw data of Fig. 3, local density of states above Cl atoms, artificial flattening of the buckling, and results of NaCl on Ag, which includes Ref. [39].
- [24] M. Pivetta, F. Patthey, M. Stengel, A. Baldereschi, and W.-D. Schneider, Local work function Moire pattern on ultrathin ionic films: NaCl on Ag(100), *Phys. Rev. B* **72**, 115404 (2005).
- [25] W. Hebenstreit, J. Redinger, Z. Horozova, M. Schmid, R. Podloucky, and P. Varga, Atomic resolution by STM on ultrathin films of alkali halides: Experiment and local density calculations, *Surf. Sci.* **424**, L321 (1999).
- [26] F. E. Olsson, M. Persson, J. Repp, and G. Meyer, Scanning tunneling microscopy and spectroscopy of NaCl overlayers on the stepped Cu(311) surface: Experimental and theoretical study, *Phys. Rev. B* **71**, 075419 (2005).
- [27] M. Schneiderbauer, M. Emmrich, A. J. Weymouth, and F. J. Giessibl, CO Tip Functionalization Inverts Atomic Force Microscopy Contrast via Short-Range Electrostatic Forces, *Phys. Rev. Lett.* **112**, 166102 (2014).
- [28] A. Liebig, A. Peronio, D. Meuer, A. J. Weymouth, and F. J. Giessibl, High-precision atomic force microscopy with atomically-characterized tips, *New J. Phys.* **22**, 063040 (2020).
- [29] A. Liebig, P. Hapala, A. J. Weymouth, and F. J. Giessibl, Quantifying the evolution of atomic interaction of a complex surface with a functionalized atomic force microscopy tip, *Sci. Rep.* **10**, 14104 (2020).
- [30] G. Kresse and J. Furthmuller, Efficient iterative schemes for *ab initio* total-energy calculations using a plane-wave basis set, *Phys. Rev. B* **54**, 11169 (1996).
- [31] M. Dion, H. Rydberg, E. Schroder, D. C. Langreth, and B. I. Lundqvist, Van der Waals Density Functional for General Geometries, *Phys. Rev. Lett.* **92**, 246401 (2004).
- [32] K. Berland and P. Hyldgaard, Exchange functional that tests the robustness of the plasmon description of the van der Waals density functional, *Phys. Rev. B* **89**, 035412 (2014).
- [33] G. Roman-Perez and J. M. Soler, Efficient Implementation of a van der Waals Density Functional: Application to Double-Wall Carbon Nanotubes, *Phys. Rev. Lett.* **103**, 096102 (2009).
- [34] F. Mohn, L. Gross, N. Moll, and G. Meyer, Imaging the charge distribution within a single molecule, *Nat. Nanotechnol.* **7**, 227 (2012).
- [35] O. Dulub, U. Diebold, and G. Kresse, Novel Stabilization Mechanism on Polar Surfaces: ZnO(0001)-Zn, *Phys. Rev. Lett.* **90**, 016102 (2003).

- [36] M. Setvin, M. Reticcioli, F. Poelzleitner, J. Hulva, M. Schmid, L. A. Boatner, C. Franchini, and U. Diebold, Polarity compensation mechanisms on the perovskite surface $\text{KTaO}_3(001)$, *Science* **359**, 572 (2018).
- [37] F. J. Giessibl, Advances in atomic force microscopy, *Rev. Mod. Phys.* **75**, 949 (2003).
- [38] J. Martinez-Castro, M. Piantek, S. Schubert, M. Persson, D. Serrate, and C. F. Hirjibehedin, Electric polarization switching in an atomically thin binary rock salt structure, *Nat. Nanotechnol.* **13**, 19 (2018).
- [39] F. J. Giessibl, The qPlus sensor, a powerful core for the atomic force microscope, *Rev. Sci. Instrum.* **90**, 011101 (2019).